Correlation between 1064 nm laser attack and thermal behavior in STT-MRAM

Nicole Yazigy, J. Postel-Pellerin, G. Di Pendina, R.C. Sousa, V. Della Marca, Pierre Canet

Correlation between 1064nm laser attack and thermal behavior in STT-MRAM

N. Yazigy[a], J. Postel-Pellerin[a,*], V. Della Marca[a],
R. C. Sousa[b], G. Di Pendina[b] P. Canet[a]

[a] Aix Marseille University, CNRS, IM2NP, 13451 Marseille, France.
[b] SPINTEC, University Grenoble Alpes, CNRS, CEA-SPINTEC, CEA, 38000 Grenoble, France.

Abstract

In this paper, the impact of a 1064nm laser attack on a STT-MRAM cell is experimentally studied in real-time, for the first time, during reading and writing operations, in order to understand the behavior of a sensing circuit under a brutal temperature variation. This must be considered for the technology design. We highlight a reading current variation during the laser shots, that can impact the sensing circuits. The switching probability between the two states has been measured as well as the impact of the irradiation time, laser power and cell size. We correlate the results with electrical characterizations in a wide range of temperature, demonstrating the attack thermally affects the STT-MRAM behavior. In conclusion, the suitable countermeasures can be adopted.

1. Introduction

A promising non-volatile memory known as Spin-Transfer Torque Magnetic Random-Access Memory (STT-MRAM) combines a fast writing operation with a high density and significant endurance (up to 1013 cycles) [1,2]. The Magnetic Tunnel Junctions (MTJ) are composed by a CoFeB/MgO/CoFeB stack, where MgO layer serves as a tunnel barrier layer. Programming the cell from the Anti-Parallel (AP) to the Parallel (P) state and vice-versa is performed by forcing a spin-polarized current through the device. The transverse component of the spin current is absorbed in the free layer, leading to a torque induced reversal of the CoFeB ferromagnetic material magnetization known as the Spin Transfer Torque (STT) effect [3,4] as detailed in [5]. Magnetization direction is the form in which the data in MTJ is coded and its read/write latency is controlled by the stochastic nature of the reversal, device size, and current flowing through the layers [6]. An important characteristic of the MTJ is the Tunnel Magnetoresistance Ratio (TMR) defined as $(R_{AP}-R_P)/R_P$, where R_{AP} and R_P are the resistances of AP and P states respectively [7].

The goal of this study is to investigate how an infrared laser attack affects the STT-MRAM behavior during the reading and programming phases. Additionally, we also aim at understanding the physical contribution of the laser attack, which can be a thermal, or have a photoelectrical contribution [8]. To perform a quasi-static current versus voltage (I-V) loop, as shown in Fig. 1, the bias voltage is applied to the top electrode of the MTJ, with a resistance-area product R.A.~12Ω·μm^2, a TMR~100% and a diameter~100nm, while grounding the bottom electrode and measuring the top electrode current. A voltage ramp is applied to write the cell with a positive bias to switch the cell to the P state and a negative bias to switch it to the AP state. The reading voltage ($V_R = +100mV$) is chosen to determine the cell state, without modifications, and to extract the corresponding resistance value.

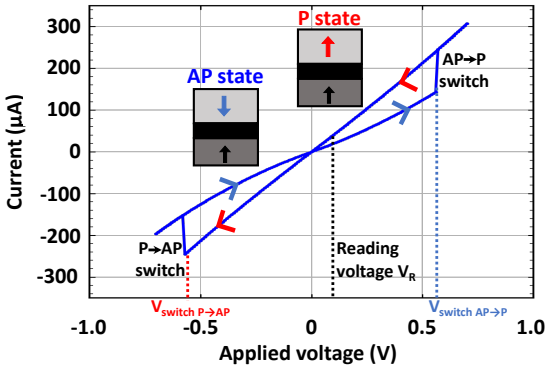

Fig. 1. Quasi-static I-V characteristic loop of state transitions of the Magnetic Tunnel Junction.

* Corresponding author. jeremy.postel-pellerin@univ-amu.fr.
Tel: +33 413 554 037

2. Results

2.1. Experimental setup description and attack methodology

In order to attack the cells while the electrical characterization is being performed, we have developed the configuration shown in Fig. 2, which enables to apply a voltage through the probes using an Agilent 4156B and a simultaneous one second laser irradiation. The laser used in this study has a wavelength of 1064nm. The maximum output peak-power is 3W focused to a diameter of 5µm corresponding to the spot size. The Tektronix AWG2005 pulse generator activates and synchronizes the measurements with the laser pulse. The light flux is injected at the wafer backside, since silicon is transparent for this wavelength, while the probes contact the STT-MRAM on the frontside. The experimental setup and methodology are detailed in [9].

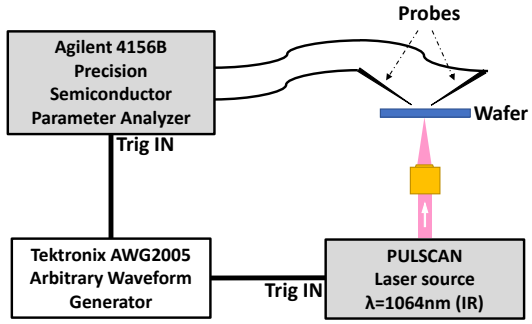

Fig. 2. Diagram of optical and electrical characterization systems.

2.2. Laser attack during the reading phase

During a standard reading operation, at a low voltage, no switch is supposed to happen. To determine the impact of the laser attack on the reading operation, we first read the current versus time while applying a reading voltage. We consider a positive V_R when AP is the initial state while a negative reading bias is used for an initial P state. Thus, the polarization is in agreement with the sign of switching operation. The impact of the value of V_R will be discussed in section 2.4. Fig. 3 shows the reading current as a function of time for various applied laser powers for an initial AP state, for the standard $V_R = +100mV$. In that case, we can observe during the irradiation an over-current increasing with the laser power (LP). However, for an initial P state and an opposite reading voltage value $V_R = -100mV$, the measured absolute current value decreases during the laser pulse, showing an under-current, visible in Fig. 4. When increasing the LP, this under-current amplitude also increases.

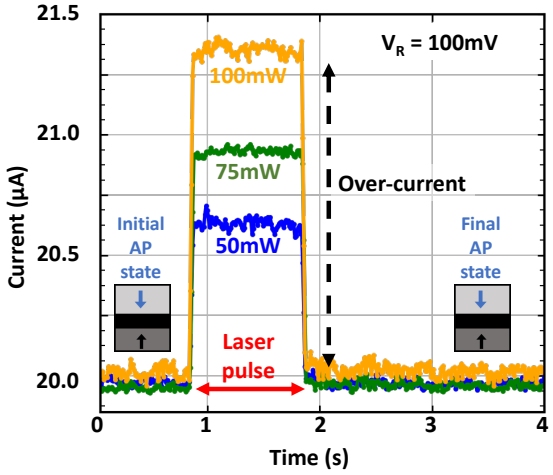

Fig. 3. Laser attack effect on the reading current as a function of time at $\boldsymbol{V_R = +100mV}$ with an initial AP state and a laser power of 50, 75 and 100mW.

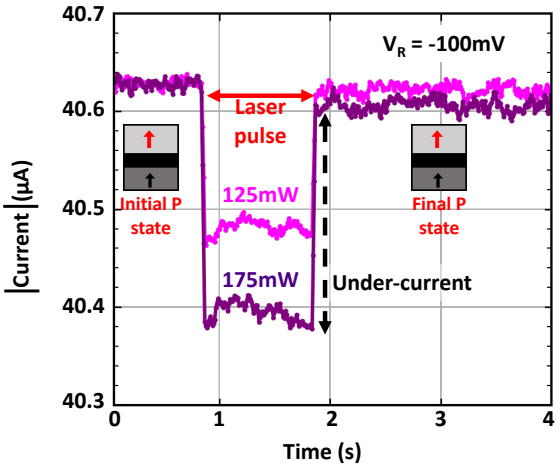

Fig. 4. Laser attack effect on the absolute value of the current as a function of time at $\boldsymbol{V_R = -100mV}$ with a P initial state and a laser power of 125 and 175mW.

2.3. State transition during laser attack

The dynamic current measurement at 125mW, black curve in Fig. 5, when reading the cell at $V_R = +100mV$ demonstrates that the cell gets enough current during a laser attack to switch from the AP to the P state. This current amount is compared with the results, carried out on the same cell, of Fig. 3 and 4, in the inset. We can notice that the switch is not instantaneous after the beginning of the laser irradiation. In the following of this paper, we will call this delay the irradiation time before switching, denoted t_L. Moreover, in the inset we show that using a laser power of 125mW, a $|V_R| = +100mV$, the same under-current level is obtained whatever the initial cell state.

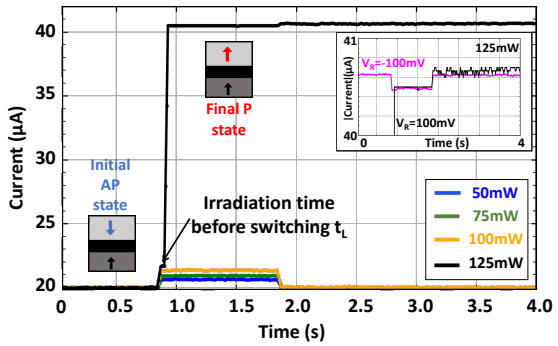

Fig. 5. Over-current and switch under laser irradiation from AP to P state at 125mW for a reading voltage $\boldsymbol{V_R = +100mV}$. In the inset we compare for a laser power of 125mW the absolute value of the current for an initial P state at $\boldsymbol{V_R = -100mV}$ to the one for an initial AP state at $\boldsymbol{V_R = +100mV}$.

2.4. Switching probability and time

Considering an initial AP state, we have repeated ten times this previous experiment for a given read voltage and progressively increase the laser power (from 50mW to 125mW). Thus, to better evaluate the cycle to cycle switching variability under the laser attack, we measured and plotted the switching probability for the same cell. This has been extracted for $V_R = 100mV$ and $V_R = 10mV$ and showed in Fig. 6. We can notice that the switching probability decreases by lowering the read voltage for a constant laser power. We can fit these switching probabilities using Gaussian distributions for $V_R = 10mV$ and $100mV$ with respective standard deviations of 7 and 10mW and respective means of 113.5 and 106mW. Moreover, for an initial P state, the transition to the AP becomes possible. Using a negative bias and a LP of 300mW, a 10% of switch probability has been extracted. Nevertheless, this power level induces a cell degradation as previously presented [9], demonstrating the higher stability of the parallel state.

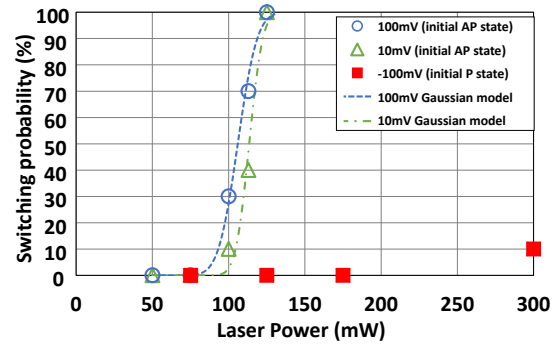

Fig. 6. Measured switching probabilities of a STT-MRAM cell due to laser attack (marks) and their corresponding Gaussian distributions (dashed lines).

The impact of the reading voltage on the irradiation time before switching (t_L) is plotted in Fig. 7, for a laser power of 125mW at which the switching probability is equal to 100% for all bias conditions. The t_L decreases when the read voltage increases. In Fig. 7 we present the ten measurements (full marks) and their mean value (open marks) at each reading voltage. It is worth to notice that the sampling time during measurements was fixed at 4ms, lower than the extracted values for the irradiation time. The irradiation time t_L tends to saturate increasing the reading voltage, the description of this behavior will be presented in section 3.

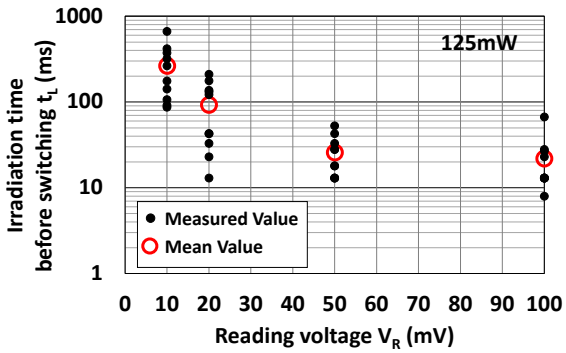

Fig. 7. Impact of the reading voltage $\boldsymbol{V_R}$ on the irradiation time before switching $\boldsymbol{t_L}$ for a laser power of 125mW for ten measurements at each bias condition.

2.5. Impact of the device size

In order to study the laser switching variability between different cells, we chose 3 cells with different current values in AP state (I_{AP}) extracted at $V_R = +100mV$, for different cell areas assuming a constant R.A. product. Fig. 8 shows the mean values of ten over-current responses during the irradiation pulse as a function of the laser power. We also highlight by cross marks the value from which there is a 50% chance of switching the cell from the AP to the P state. This threshold level of over-current is 1.4, 1.7 and 1.9µA, corresponding to a LP of 105, 75 and 65mW for cells 1, 2 and 3 respectively. It is therefore possible to plot in Fig. 9, the slopes of the trend curves as a function of the current in AP state, that are well described by a linear decrease. The switching threshold is also plotted in Fig. 9 as a function of the AP state current also confirming a linear decrease.

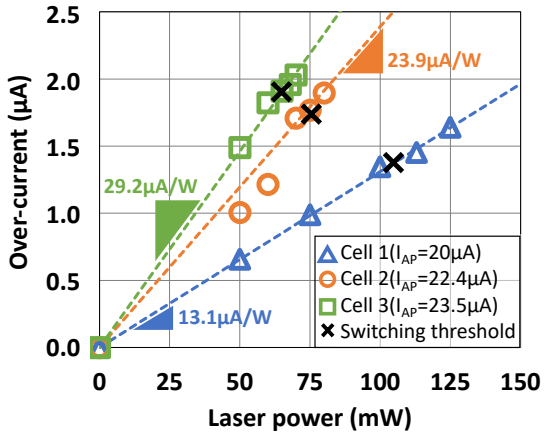

Fig. 8. Over-current, for three different cells, during laser pulse at $\boldsymbol{V_R = 100mV}$ as a function of the laser power (mean values for ten measurements). The switching threshold is extracted at 50% of switching probability.

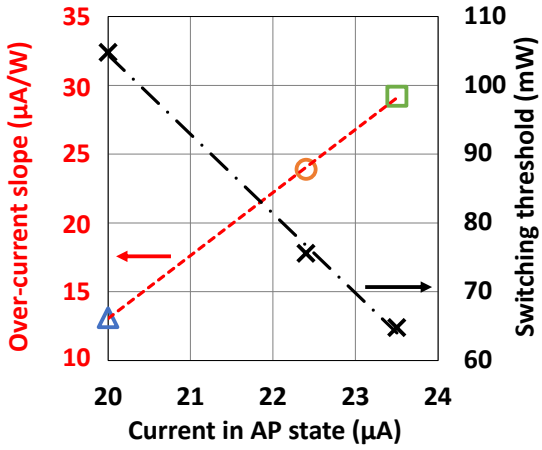

Fig. 9. Over-current trendline slope (left axis) and the threshold laser power (right axis) as a function of the AP state current (I_{AP}).

2.6. Comparison between laser attack and temperature effect during the programming phase

During the complete programming phase, I-V loops illustrated in Fig. 1, the laser attacks were applied covering the entire duration of the cycle. The cell resistance versus applied voltage (R-V) characteristics have been extracted by varying the laser power. We observed a variation in the programming window of the cell as shown in Fig. 10. As mentioned in section 2.1, the laser attack is performed on the backside, thus facing a 500nm SiO2 layer on which the STT-MRAM stack is fabricated, which is supposed to prevent the MTJ from induced photocurrents. Thus, the effect of the laser should be mainly thermal. To confirm this hypothesis, a thermal characterization was performed on the cell by heating the chuck of the probe station from 25°C to 105°C, as described in a previous study [10]. The obtained results are presented in Fig. 11, showing very similar behaviors with the ones obtained in Fig. 10 under the laser irradiation.

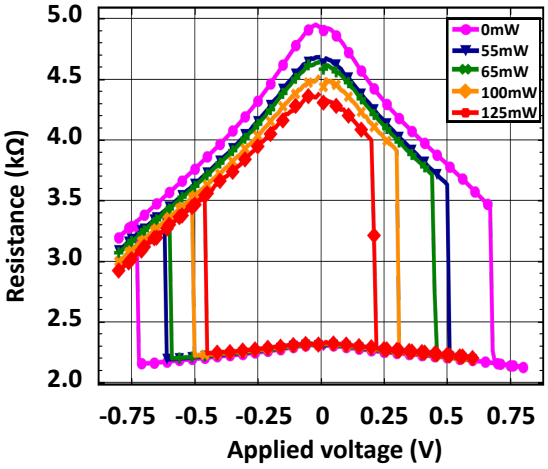

Fig. 10. Laser power variation on the quasi-static R-V characteristics during the programming cycle.

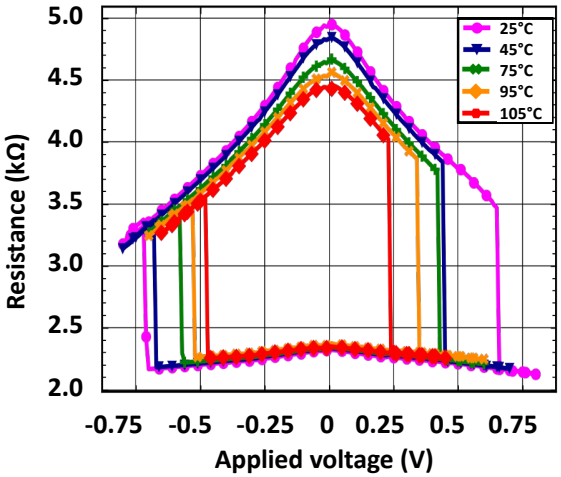

Fig. 11. Temperature effect on the quasi-static R-V characteristics during the programming cycle.

The comparison between the effect of the laser attack and the variation of the temperature (T) is firstly obtained by extracting from Fig. 10 and 11 the values of the two resistances for the P and AP states at $V_R = +100mV$, plotted in Fig. 12 and 13. We notice that there is a significant modification in the resistance of the AP state compared to the weak variation of the P state resistance. We stopped the experiments at 125mW of LP that represents the limit to obtain de 100% switching probability from the AP to P state.

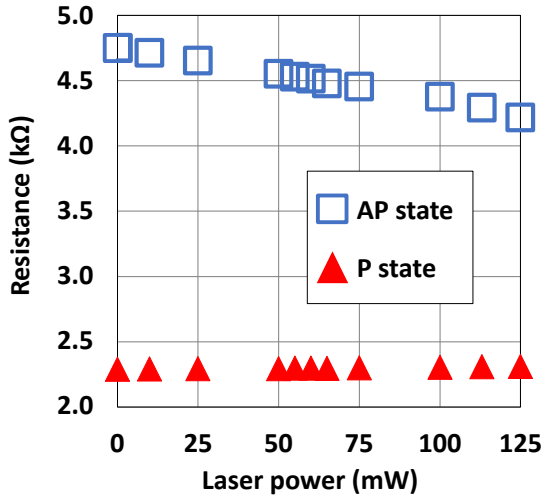

Fig. 12. Effect on the cell resistances of the laser power during the programming phase.

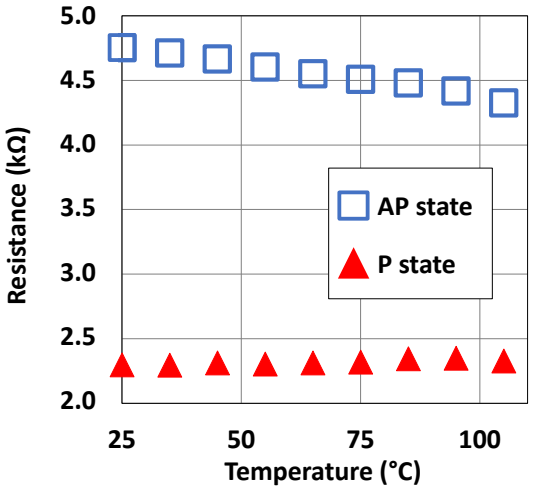

Fig. 13. Effect on the cell resistances of the temperature during the programming phase.

From Fig. 10 and 11 we can also extract and plot the switching voltages of the two transitions, AP→P and P→AP, presented in Fig. 14 and 15. Here we point the fact on the non-symmetric variation of these V_{switch} values. Hence, the limit in terms of LP and T is fixed by the condition: $V_R < V_{\text{switchAP}\to\text{P}}$.

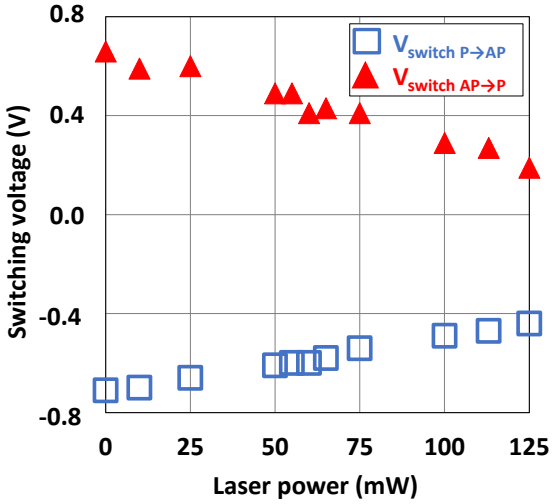

Fig. 14. Effect on the cell switching voltages of the laser power during the programming phase.

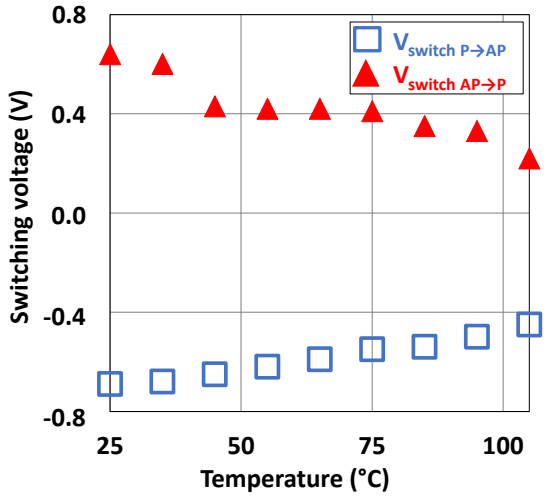

Fig. 15. Effect on the cell switching voltages of the temperature during the programming phase.

3. Discussion

Clearly, from Fig. 14 and Fig. 15, we can conclude that the impact of the laser irradiation can be fully explained as a thermal effect in the MTJ, while the incidence of an induced photocurrent can be neglected. To deeply correlate the consequence of a laser irradiation with the temperature enhancement we calculate the programming window (ΔV) as the difference: $\Delta V = V_{\text{switch AP}\to\text{P}} - V_{\text{switch P}\to\text{AP}}$. The linear variation of ΔV as function of LP and T is plotted in Fig. 16 and Fig. 17 respectively.

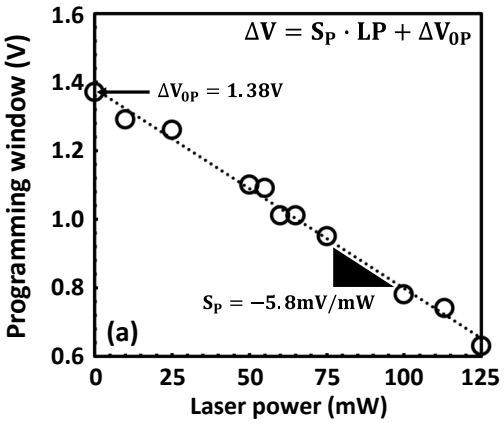

Fig. 16. The switching voltages difference as a function of the laser power.

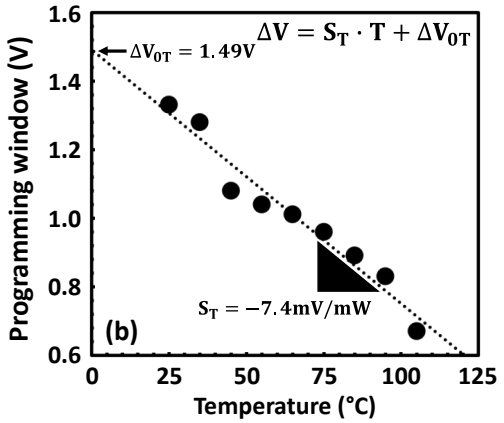

Fig. 17. The switching voltages difference as a function of the temperature.

Where S_P, S_T represent the slopes and $\Delta V_{0P}, \Delta V_{0T}$ indicate the intercepts of the two lines. Hence, ΔV represents the link between LP and T leading to the possibility of modeling the dependency between these parameters as shown in Fig. 18.

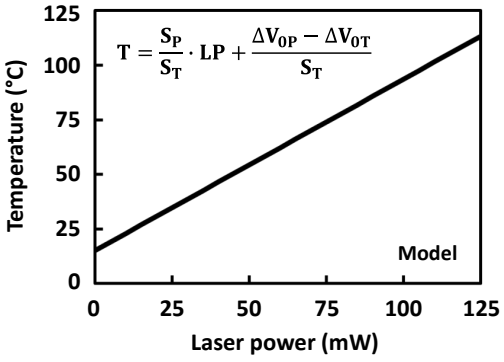

Fig. 18. Correlation between the temperature in the MTJ and the laser power.

In this case, even if the exact temperature in the MTJ during the irradiation is not predicted, the memory cell functioning in a circuit under laser attack can be emulated.

The overcurrent behavior (+10% at 125mW) in Fig. 3 is coherent with the resistance decrease of the AP state with increasing temperature (Fig. 9), which appears with laser heating. Therefore, Fig. 9 shows a weak increase of P resistance with temperature, which explains the under-current (-0.4% at 125mW) in Fig.3. Hence, the laser heating explains both behaviors (over- and under-current).

The irradiation time before switching (t_L) strongly decreases with increasing reading voltage as the preswitching time in another cell [5,10]. By decreasing the reading voltage at a given laser power, the energy received by the cell is reduced and its switching probability consequently decreases. Therefore, the temperature changes the resistance [11] and subsequently the current that corresponds to a given voltage. Thus, for larger surface cells, more laser power, and hence heat, is needed to initiate switching. Then we can notice a saturation effect of $t_L \sim 20$ms. This can be due to the programming window closure, that enables the reading voltage approaching the AP to P switching voltage.

According to existing studies on the temperature dependence of similar perpendicular anisotropy junctions in a range of -183 to 27°C [12], TMR shows a linear decrease as the temperature increases, up to a point where TMR is near zero, at which stage too many thermal fluctuations in the free layer cause the spin polarization to vanish. The main temperature effect on MTJ resistance is mostly on the AP state, with variations of the parallel state R_P limited to a few percent in a large temperature range. In contrast, for the AP state thermal phonons across the barrier, as the temperature increases, results in a growing magnetic disorder reducing the R_{AP} [13].

In perpendicular anisotropy systems, there is also a drop in effective spin polarization with a decrease in effective perpendicular anisotropy created by the temperature increase. On the other hand, planar structures can also exhibit DC bias dependence, which also influences effective spin polarization and the R_{AP} value, indicating the underlying relationship between TMR bias dependence and tunnel barrier properties. The spin excitations localized at the interface between the magnetic electrodes and the tunnel barrier may also be the cause of this bias dependence of TMR [14, 15].

We can also highlight that the impact of the laser attack on the STT-MRAM behavior (switch from AP to P state, over-current during reading, variation of resistance levels and switching conditions) could also

affect the behavior of any circuit embedding these devices. In particular, this study is part of the MISTRAL project, aiming at designing a hybrid MRAM/CMOS-based implementation of a LightWeight Cryptography (LWC) algorithm (Ascon cipher) for IoT applications [16] and the effects we observed will be included in the full algorithm design and simulation to implement countermeasures.

4. Conclusion

The effect of a 1064nm laser on the STT-MRAM is studied as well as its effect on the temperature variation of the MTJ. We present here the cell current variation during the laser irradiation in a reading condition for different laser powers. The establishing of an over- or under-current, depending on the sign of the reading voltage, can impact the sensing circuits used to read the cell, or in a hybrid circuit configuration. This must be considered for the technology design. To deep understand the cell behavior, we verified it is possible to reach a cell switching from an AP to P state without degradation. The reading voltage and the irradiation time, as well as the cell size, impact the switching probability and must be taken into account to find a countermeasure method. Finally, we demonstrate the direct correlation between the laser power and temperature showing the reduction of the programming window as a function of these two physical aspects. It is thus possible to emulate a laser attack considering the electrical model variations in a wide range of temperature.

Acknowledgements

The authors would like to thank Ecole des Mines de Saint-Etienne in Gardanne for providing access to the advanced laser test bench. This work was supported by the grant n°ANR-19-CE39-0010 (MISTRAL Project) overseen by the French National Research Agency (ANR).

References

[1] M. Kharbouche-Harrari, et al., “MRAM: from STT to SOT, for security and memory,” Conference on Design of Circuits and Integrated Systems, 2018.
[2] M. H. Kryder and S. K. Chang, “After Hard Drives—What Comes Next?,” IEEE Transactions on Magnetics, 45(10), 3406–3413, 2009.
[3] J. Chatterjee, et al., ”Physicochemical origin of improvement of magnetic and transport properties of STT-MRAM cells using tungsten on FeCoB storage layer,” Applied Physics Letters, 2019.
[4] D. Apalkov, et al., “Magnetoresistive Random Access Memory,” Proceedings of the IEEE, vol. 104, pp. 1796–1830, 2016.
[5] N. Yazigy, et al., “Real-time switching dynamics in STT-MRAM,” IEEE Journal of the Electron Devices Society, 2022.
[6] A. Iyengar, et al., “Side channel attacks on STTRAM and low-overhead countermeasures,” IEEE International Symposium on Defect and Fault Tolerance in VLSI and Nanotechnology Systems (DFT), 2016.
[7] J. S. Moodera, et al., “Large magnetoresistance at room temperature in ferromagnetic thin film tunnel junctions,” Phys. Rev. Lett, 1995.
[8] Y. Xu, et al., “Laser powered magnetic-random access memory,” IEEE Magnetics Conference (INTERMAG), 2015.
[9] N. Yazigy, et al., “Real-time electrical measurements during laser attack on STT-MRAM,” International Conference on Microelectronic Test Structures, March 2023, to be published.
[10] N. Yazigy, et al., “Experimental analysis on stochastic behavior of preswitching time in STT-MRAM,” Microelectronics Reliability, Volume 138, 2022.
[11] Y. Wang, et al. “Compact thermal modeling of spin transfer torque magnetic tunnel junction,” Microelectronics Reliability, 2015.
[12] A. Timopheev, et al., “Inhomogeneous free layer in perpendicular magnetic tunnel junctions and its impact on the effective anisotropies and spin transfer torque switching efficiency,” Physical Review B, 2017.
[13] S. S. P. Parkin, et al., ”Giant tunnelling magnetoresistance at room temperature with MgO (100) tunnel barriers,” Nature Materials, 2004.
[14] S. Zhang, et al., ”Quenching of Magnetoresistance by Hot Electrons in Magnetic Tunnel Junctions,” Physical Review Letters, 1997.
[15] J. J. Sun, et al. “Tunneling magnetoresistance and current distribution effect in spin-dependent tunnel junctions,” Journal of Applied Physics, 1998.
[16] N. Roussel, et al. “CMOS/STT-MRAM Based Ascon LWC: a Power Efficient Hardware Implementation,” IEEE International Conference on Electronics, Circuits and Systems (ICECS), 2022.